processes

MDPI

Article

Reservoir Architecture of Turbidite Lobes and Remaining Oil Distribution: A Study on the B Formation for Z Oilfield of the Illizi Basin, Algeria

Changhai Li [1], Weiqiang Li [2,*], Huimin Ye [1], Qiang Zhu [1], Xuejun Shan [1], Shengli Wang [1], Deyong Wang [1], Ziyu Zhang [3], Hongping Wang [2], Xianjie Zhou [1] and Zhaofeng Zhu [1]

[1] Sinopec International Petroleum Exploration and Development Corporation, Beijing 100029, China; chhli.sipc@sinopec.com (C.L.)
[2] PetroChina Hangzhou Research Institute of Geology, Hangzhou 310023, China
[3] Department of Chemical Engineering and Analytical Sciences, The University of Manchester, Manchester M13 9PL, UK
* Correspondence: liwq_hz@petrochina.com.cn; Tel.: +86-0571-87671206

Abstract: The turbidite lobe is a significant reservoir type formed by gravity flow. Analyzing the architecture of this reservoir holds great importance for deep-water oil and gas development. The main producing zone in Z Oilfield develops a set of turbidite lobes. After more than 60 years of development, the well spacing has become dense, providing favorable conditions for detailed research on reservoir architecture of this kind. Based on seismic data, core data, and logging data, combined with the results of reservoir numerical simulation, this paper studies the reservoir architecture of turbidite lobes, displays the distribution of remaining oil in the turbidite lobes, and proposes development policies suitable for turbidite lobe reservoirs. The results show that the turbidite lobes can be classified into four sedimentary microfacies: lobe off-axis, lobe fringe, interlobe facies, and feeder channel facies. The study area is mainly characterized by multiple sets of lobes. There are feeder channels running through the south to the north. Due to the imperfect well pattern, the remaining oil is concentrated near the lobe fringe facies and the gas–oil contact. It is recommended to tap the potential of the turbidite lobes by adopting the "production at the off-axis lobes facies and injection at the lobe fringe facies (POIF)". The study on the reservoir architecture and remaining oil of turbidite lobes has crucial guiding significance for the efficient development of Z Oilfield and can also provide some reference for developing deep-water oilfields with similar sedimentary backgrounds.

Keywords: turbidite lobes; reservoir architecture; remaining oil; B Formation; Z Oilfield

check for updates

Academic Editor: Dicho Stratiev

Received: 26 January 2025
Revised: 15 February 2025
Accepted: 17 February 2025
Published: 10 March 2025

Citation: Li, C.; Li, W.; Ye, H.; Zhu, Q.; Shan, X.; Wang, S.; Wang, D.; Zhang, Z.; Wang, H.; Zhou, X.; et al. Reservoir Architecture of Turbidite Lobes and Remaining Oil Distribution: A Study on the B Formation for Z Oilfield of the Illizi Basin, Algeria. *Processes* **2025**, *13*, 805. https://doi.org/10.3390/pr13030805

Copyright: © 2025 by the authors. Licensee MDPI, Basel, Switzerland. This article is an open access article distributed under the terms and conditions of the Creative Commons Attribution (CC BY) license (https://creativecommons.org/licenses/by/4.0/).

1. Introduction

Turbidite lobes represent a crucial type of oil and gas reservoir, and a comprehensive understanding of their architecture is of utmost importance. Reservoir architecture studies involve an in-depth exploration of the reservoir's internal structure, taking into account aspects such as scale, shape, and the combinatorial relationships among various constituent units [1,2]. The research on reservoir architecture bears significant guiding implications for the investigation of remaining oil distribution. This is especially true for oilfields in the middle and late development stages, as it provides essential insights for potential tapping and enhanced oil recovery. Therefore, many previous workers made efforts to study the reservoir architecture of turbidite lobes. Jamil [3], Mueller [4], and Zakaria [5]

studied the sedimentary facies, facies association, and reservoir architecture of turbidite lobes based on outcrop data. J. Bourget et al. [6] used the seismic data to research the architecture of modern sedimentary lobes and divided the lobes into proximal, middle, and distal lobe areas. Doughty-Jones et al. [7] displayed the reservoir architecture of the ponded intraslope basin and put forward that the lobe shape and spatial location are driven by the response of the lobes to topographic growth along the edge of the basin and inherited seabed relief generated by previous lobe growth. Zhang and Li [8] took the Carboniferous outcrop in Clare Basin, Ireland as an example to analyze the architecture and three-dimensional distribution characteristics of turbidite lobes which is massive sandstone in the proximal end to thinner sandstone and mudstone interbeds from axis to fringe. Duan RK et al. [9] took the Miocene D oil formation in the Akpo Oilfield in the Niger Delta Basin as an example to study the overlapping relationship of different units of the turbidite lobes. T. Spychala et al. [10], Prelat et al. [11], and Zhang et al. [12] carried out quantitative statistics on the distribution scale of turbidite lobes and they built the width vs. maximum thickness for different depositional environment. A. Siddiqui et al. [13] displayed the lateral connectivity of turbidite lobes using the two-dimensional modeling method. Groenenberg et al. [14] used a process-based numerical model to simulate the vertical stacking evolution characteristics of turbidite lobes. A. Macdonald et al. [15] proposed a six-stage model for lobe-element evolution that documents successive phases of deposition, sediment bypass, erosion, and lobe abandonment. Starek and Fuksi [16] built the overlapping model of different lobes and pointed out that there are four kinds of bed thickness patterns in lobes instead of thickening-upward patterns only. T. Spychala et al. [17] compared sedimentary facies, architecture, and flow processes between frontal and lateral submarine lobe fringes. Zhang et al. [18] displayed the controlling effect of sea level change on the formation of turbidite lobes geometry based on seismic data. A fuhrmann et al. [19] discussed the bottom current modification for turbidite lobes. Gervais et al. [20] presented the pre-existing morphology controls on the three-dimensional geometry of the lobes. Kuswandaru et al. [21] verified that hybrid event beds in lobe proximal locations through deflection and deceleration of incoming flows by confining counter slopes. Zakaria et al. [5] established a sedimentary model of turbidite lobe and sedimentary environment based on outcrop data. Zhang et al. [22] demonstrated that marine turbidite lobes and large lacustrine turbidite lobes are similar. Mutti et al. [23] systematically reviewed key issues related to turbidite lobes, including concepts, submarine flow mechanisms, spatial distribution characteristics, and sedimentary sequences.

In recent years, research on turbidite lobes has been bifurcated into two primary focal areas. The first area of focus is the in-depth exploration of sedimentary characteristics. Q. Liu et al. [24] carried out a meticulous comparison between the depositional architectures of unconfined and confined turbidite lobes. Their findings revealed that in unconfined systems, sandstone bodies assume lobate morphologies and exhibit self-organization. Conversely, within confined systems, individual beds possess planform geometries that align with basin geometries and stack vertically. This vertical stacking gives rise to simple "sheet-like" architectures, characterized by negligible variation in facies association. E. Scacchia et al. [25] presented compelling evidence for the presence of supercritical bedforms in two distinct settings: within the scour of an erosional cyclic step and on the stoss side of a depositional cyclic step or antidune within a confined deep-sea fan lobe. P. Łapcik [26] highlighted that for turbidite lobes, the deposition of structured sandstone–mudstone sequences gradually increases from the proximal to the distal regions. L. A. Gonçalves et al. [27] unearthed the sedimentary processes of turbidite lobes by applying the high-resolution sequence stratigraphy method. J. F. Cabrera-Ortiz et al. [28] demonstrated that the abundance of fossils steadily decreases from the proximal fan to the distal fan. The

second major area of research pertains to the in-depth investigation of the distribution and connectivity of lobe reservoirs, as well as the development of geological modeling methods. D. Fernandes et al. [29] proposed leveraging a convolutional neural network to calculate seismic impedance inversion, with the aim of enhancing the resolution of seismic data. S. Obafemi et al. [30] established a novel method for predicting the distribution of turbidite lobes. Their approach involves employing an unsupervised artificial neural network, which analyzes seismic data to map out the likely locations of these lobes. O. Olagundoye et al. [31] put forward a method that utilizes detuned seismic amplitudes to predict the net-to-gross ratio. O. Alpak et al. [32] pointed out that the lobe axis permeability, the extent of shale-drape coverage, and the chosen well spacing are the principal factors that govern the connectivity of turbidite lobes. H. Lim et al. [33] demonstrated that compensational stacking leads to extensive overlaps between lobe element layers. These overlaps play a significant role in enhancing lateral reservoir connectivity. S. Silveira et al. [34] verified that the Indicator Simulation technique is highly efficient in accurately describing the characteristics of turbidite lobes. R. Xu et al. [35] developed a multiple-point stochastic methodology. This approach enables the precise characterization of the architecture of turbidite lobes and effectively depicts their superposition distribution features, providing a more comprehensive understanding of the spatial arrangement of these geological structures. Previous research efforts have predominantly concentrated on the investigation of the reservoir architecture within turbidite lobes themselves. However, a conspicuous gap persists in the discourse regarding the impact exerted by the reservoir architecture of turbidite lobes on the distribution of remaining oil.

The Oilfield is an important oil play located at the southeast of Algeria. The main pay zone of Z Oilfield develops a set of Devonian turbidite sandstone [36]. After more than 60 years of development, the oilfield has experienced several stages of development strategy adjustments, and the distribution of remaining oil is extremely complex. So far, more than 340 wells have been drilled in the oilfield with a well spacing of 300 m. The dense well pattern provides a data basis for studying the reservoir architecture of turbidite lobes and its influence on the distribution of remaining oil [37]. Previous investigations of this oilfield have principally centered around sedimentary facies [38,39] and oil production [40], Nevertheless, no pertinent analyses have been carried out regarding the reservoir architecture of turbidite lobes. The analysis of the reservoir architecture of turbidite lobes assumes profound guiding significance in elucidating the controlling mechanisms of turbidite lobes over the remaining oil and in effectively tapping the remaining oil potential. At the same time, this study has important implications for the development of turbidite lobe reservoirs in the Atlantic [41,42] and the South China Sea [43].

Based on the core, logging, and seismic data in the study area, this paper applies the theory of reservoir architecture hierarchy analysis to study the reservoir architecture of turbidite lobes using the dense well pattern. We aim to clarify the control of reservoir architecture of turbidite lobes on the distribution of remaining oil, providing guidance for oilfield development.

2. Geological Background

The Illizi Basin is situated in the southeast of Algeria, having an irregular diamond shape. It measures 500 km in length from east to west and 450 km in width from north to south, with a total area of 25 × 104 km^3 (Figure 1) [44]. This basin is an important oil-bearing basin in Algeria, boasting recoverable resources of 700 million tons of crude oil and 1 trillion cubic meters of natural gas [45].

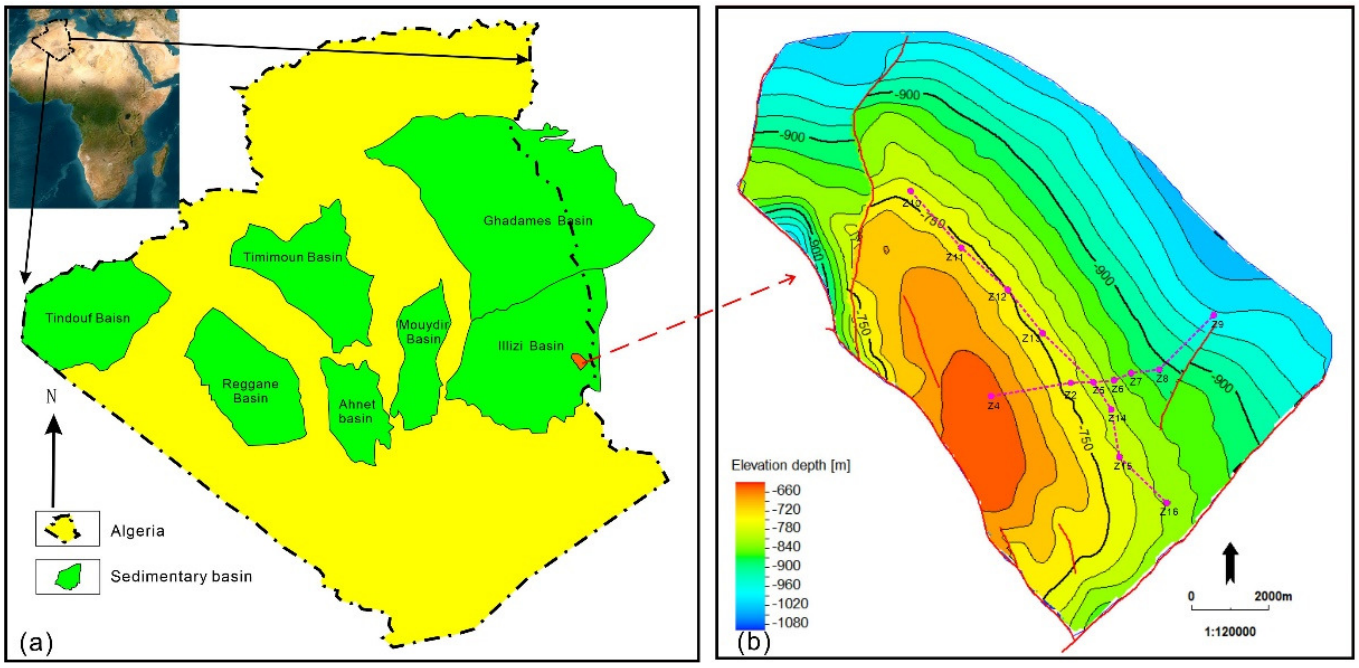


Figure 1. Location and structural characteristics of Z Oilfield. (**a**) Location of Z Oilfield; (**b**) Structural characteristics of Z Oilfield.

The Z Oilfield lies on the eastern margin of the Illizi basin. It is a faulted anticline structural reservoir with an average dip angle of approximately 3~4 degrees. The target layer is the Devonian B layer, which is a set of deep-water turbidite lobe deposits in the context of a passive continental margin with large-scale continuous sand body distribution (Figure 2) [37]. The reservoir has good petrophysical properties, with an average porosity of 21.1% and an average permeability of 182 mD [46]. It is divided into five oil zones from bottom to top: I, II, III, IV, and V. Among them, I, II, III, and IV are the main development layers and also the target layers for this study. The oilfield was put into production in 1959; after more than 60 years of development, it has experienced several development stages, including natural energy development, water injection outside the oil edge, water injection inside the oil edge, and adjustment of development layers.

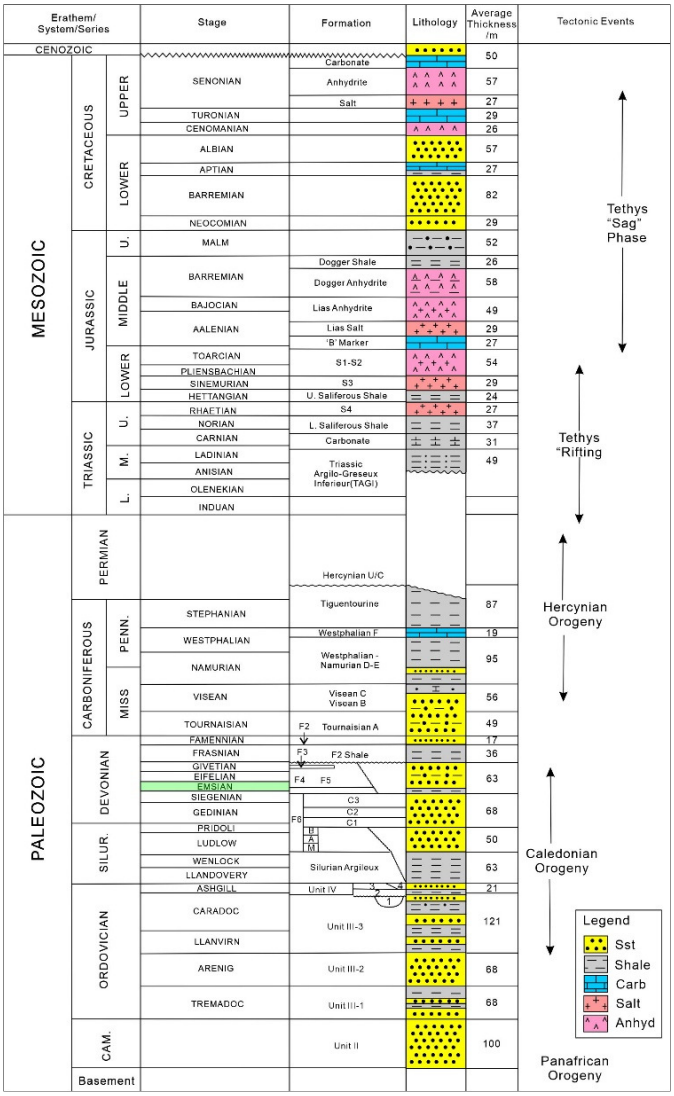


Figure 2. Stratigraphic column of Illizi Basin (adapted from [47]).

3. Methods

Core data were collected from wells Z1 and Z2. In both wells, continuous coring was carried out throughout the entire wellbore section of the target layer, with a cumulative coring length reaching 72.4 m. The core data were utilized to characterize the lithofacies and microfacies. Moreover, logging data from 334 wells were amassed, serving as the foundation for analyzing the quantitative distribution characteristics of the turbidite lobes. The seismic data acquisition and processing were completed in 2016. The panel size was set at 10 × 10 m, and the sampling rate was 2 ms. The dominant frequency of seismic data is 27 Hz. This seismic data acquisition and processing approach ensured the collection of high-quality data, which is essential for subsequent detailed geological interpretation and reservoir characterization studies. The seismic data were processed using Root Mean Square amplitude to identify the distribution of the lobes.

By making use of the gamma ray (GR) logging data from Well Z1, the wavelet transform module in MATLAB 2017 is utilized to perform wavelet transform analysis. The primary objectives of this analysis are to ascertain the sea level changes within the study area and to classify the reservoir architecture levels. The advantage of this approach lies in its ability to offer a higher resolution for the high–frequency cyclic variations in sea level and stratigraphy. This high-resolution analysis enables a more precise understanding

of the intricate relationships between sea level fluctuations and the internal structure of the reservoir.

Lithofacies analysis was conducted by utilizing core data, and sedimentary microfacies were identified. Drawing on the results of core-based sedimentary microfacies identification and integrating with the well logging data in the study area, a chart for identifying sedimentary microfacies from well logging data was established. This chart aims to offer guidance for the identification of sedimentary microfacies by means of well logging data. The quantitative distribution characteristics of different types of sedimentary microfacies were statistically analyzed using the dense well pattern.

There are numerous wells in the study area with a small spacing of only 300 m. Hence, a deterministic modeling approach is adopted to establish a geological model displaying the sedimentary microfacies distribution. Property models such as porosity, permeability, and saturation were established based on sequential Gaussian simulation. Reservoir numerical simulation was conducted based on actual reservoir parameters such as high-pressure physical properties, relative permeability curves, actual development plans, and oil and water well production systems to clarify the distribution characteristics of the remaining oil in the study area.

By comparing the distribution characteristics of the remaining oil with the sedimentary microfacies results, the controls of sedimentary facies on the distribution of the remaining oil were clarified. Reasonable strategies for tapping the potential of the remaining oil were put forward. The rationality of these strategies was confirmed by using the actual production data.

4. Results

4.1. Classification Scheme of Turbidite Reservoir Architecture

So far, there is no unified standard for the classification scheme of turbidite sandstone reservoir architecture. Some researchers have put forward classification schemes for the turbidite sandstone reservoir architecture. For instance, Mutti et al. [48] divided the turbidite sandstone reservoir architecture into five levels, and Lamb et al. [49] divided it into six levels. Majority of the researchers refer to the classification system of fluvial facies architecture units by Miall [1] to establish the classification scheme of deep-water turbidite sandstone reservoir architecture levels. For example, Lin et al. [50] put forward a seven-order division scheme for turbidite lobes, and Zhang et al. [8] proposed a seven-order division scheme from laminae to turbidite system on the basis of a detailed summary of the previous schemes of reservoir architecture of turbidite lobes (Table 1). Based on the previous classification schemes, this paper put forward a classification scheme of seven-order reservoir architecture for turbidite lobes (Figure 3). The previous classification scheme of reservoir architecture employed concepts such as “3rd–order lobe” and “Certain sedimentary interval within a single lobe”. However, without detailed explanations, it is unclear what these terms specifically refer to. In contrast, the classification scheme of reservoir architecture proposed in this paper overcomes these shortcomings. It endeavors to describe the scale and characteristics of reservoir architectures of different orders. As a result, from this new scheme, we can easily understand the sequence and characteristics of different reservoir architectures. In this study, one fifth-order reservoir architecture unit, two fourth-order reservoir architecture units, and six third-order architecture units were identified (Figure 3).

Table 1. Classification scheme of reservoir architecture.

	This Paper	Zhang [8]	Lin [50]
7th-order	Submarine fan complex	Turbidite system	Submarine fan complex
6th-order	Single submarine fan	Submarine fan	Single submarine fan, lobe complex
5th-order	Lobe system	Lobe complex	Composite lobe
4th-order	Composite lobe	4th-order lobe	Singe lobe
3th-order	Singe lobe	3rd-order lobe	Certain sedimentary interval within a single lobe
2nd-order	Single sandstone layer	Single sandstone layer	Certain rhythm unit within the sedimentary interval
1st-order	Laminae	Laminae	Laminae

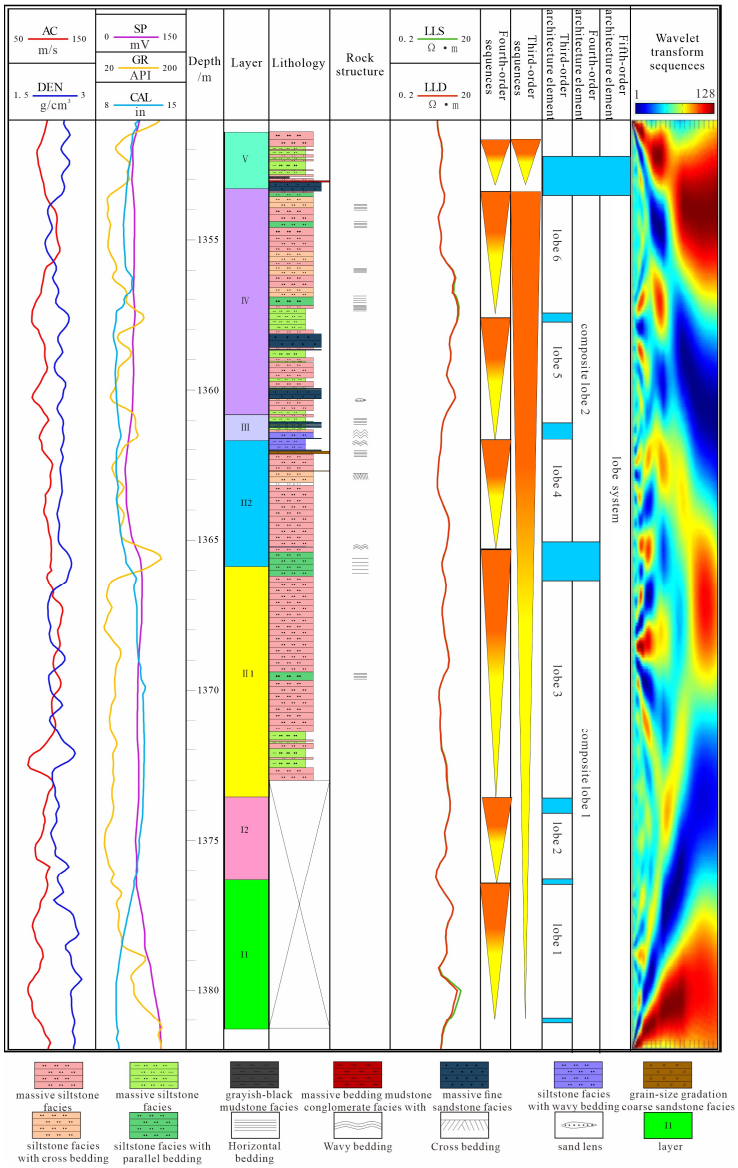


Figure 3. Comprehensive colume of Formation B in Z Oilfield.

4.2. Analysis of Reservoir Architecture of Turbidite Lobes

The study of second-order reservoir architecture holds great significance for understanding the heterogeneity of lobe reservoirs and conducting in-depth analysis of the remaining oil within lobe reservoirs. The key to analyzing the second-order reservoir

architecture of turbidite lobes lies in clarifying the characteristics of different sand bodies and their relationships. Since the second-order reservoir architecture of turbidite lobes is composed of single sand bodies, the distribution of mudstone between single sand bodies is extremely unstable, which leads to it being difficult to count the number of second-order reservoir architectures of turbidite lobes. Conducting sedimentary microfacies analysis is an effective method for analyzing the second-order reservoir architecture of turbidite lobes. In this paper, sedimentary microfacies are studied in detail using core, logging, and seismic data. Three sedimentary microfacies are mainly developed in the study area, including lobe off-axis, lobe fringe, interlobe, and feeder channel facies.

The lobe off-axis facies are the central part of deposition. The sand bodies are thick and vertically overlapped with each other. Massive bedding mudstone conglomerate lithofacies, massive bedding fine sandstone lithofacies, and massive bedding siltstone lithofacies are developed from bottom to top in the core. The massive bedding mudstone conglomerate at the bottom is the product of slump deposition, and this section is often missing. Massive bedding fine sandstone facies and massive bedding siltstone are the main sediments (Figure 4a,b). The response of these sedimentary microfacies on the GR curve is box-shaped with medium and high amplitude, and the curve is relatively smooth with few serrations (Figure 5a,b). The lobe fringe is the edge part of the turbidite lobes. Massive bedding mudstone conglomerate lithofacies, massive bedding fine sandstone lithofacies, and sandstone–mudstone interbedded lithofacies are developed from bottom to top in the core, with sand–mudstone interbedded facies as the main lithofacies (Figure 4c). These sedimentary microfacies are box-shaped or finger-shaped with serrations on the GR logging (Figure 5a,b). Interlobe facies mainly developed mudstone. The GR logging of these sedimentary facies is a mudstone baseline. Feeder channels develop in the turbidite lobes to provide a sedimentary supply for the lobes. In the core, there are gravelly siltstone lithofacies, lenticular bedding siltstone lithofacies, and massive bedding siltstone lithofacies (Figure 4d,e). Previous workers divided the feeder channels into sedimentary channels and erosive channels. However, according to the sedimentary characteristics of the channels in the study area, we divide the feeder channels into hydrodynamic gentle channels and hydrodynamic abrupt channels. The hydrodynamic gentle channels develop sandstone deposits, but due to the short-term development of rivers, the sedimentary channels show fingers on the GR logging (Figure 5a). The hydrodynamic abrupt channel coincides with the mudstone baseline on the GR logging. Mudstone is deposited in the channel with sudden hydrodynamic weakening, which appears to coincide with the mudstone baseline on the GR logging (Figure 5b).

Spectral analysis through wavelet transformation can reflect sea level changes. Spectral values 32 to 128 can, respectively, reflect short-period and long-period changes in sea level [51–54]. The information of sea level change in the study area is confirmed by the wavelet transform of the GR curve in the study area (Figure 3). Long-term sea level changes develop at the bottom of Formation I1 and the top of Formation IV, respectively. Therefore, the top of IV is an important turning point of the sea level in the study area from falling to rising and is also an important basis for analyzing sand body architecture by leveling the top of IV. Based on sedimentary microfacies and in combination with seismic data and logging data, the lateral distribution characteristics of turbidite lobes and waterways in the study area were described. The lobes are discernible in the seismic data, and the interpretation indicates that there are three lobes within the Z4–Z9 section (Figure 6a). The amplitude seismic attribute proves to be more efficacious in the identification of these lobes (Figure 6b). By analyzing the seismic amplitude attribute along the layer in the study area, it is found that layer IV develops feeder channels in the east and south. Layers I, II, and III develop a set of feeder channels that almost run through the entire area in the central

region. In the east of the study area, one set of shorter feeder channels is developed. The logging characteristics verified the seismic amplitude attribute result (Figure 7). Previous workers pointed out that the provenance of the study area is from the south and southeast, which demonstrates the accuracy of the direction of the feeder channel in this study [55].

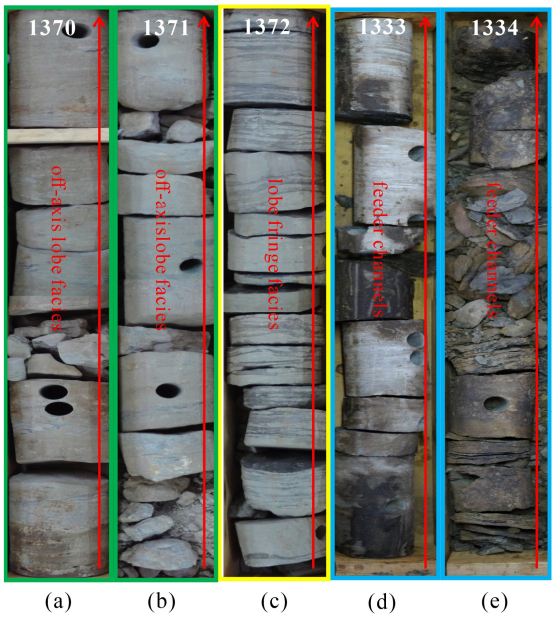


Figure 4. Core photos of different sedimentary microfacies in Formation B of Z Oilfield (**a**). Core photos of the off-axis lobes facies in the Z1 well; (**b**) Core photos of the turbidite off-axis lobes facies in the Z1 well; (**c**) Core photos of the lobe fringe facies in the Z1 well; (**d**) Core photos of the feeder channels sedimentary facies in the Z2 well; (**e**) Core photos of the feeder channels sedimentary facies in the Z2 well.

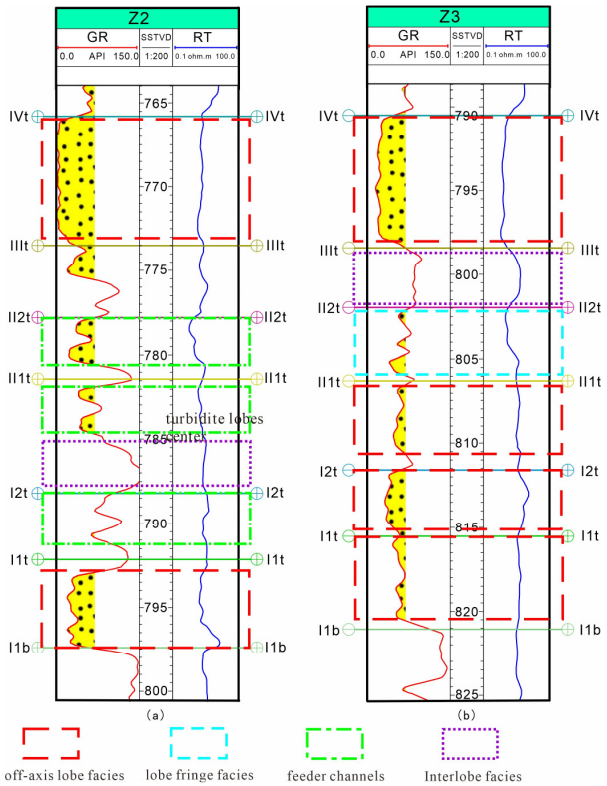


Figure 5. Logging curves features for different sedimentary microfacies. (**a**) Logging curves features for different sedimentary microfacies in Well Z2; (**b**) Logging curves feature for different sedimentary microfacies in Well Z3.

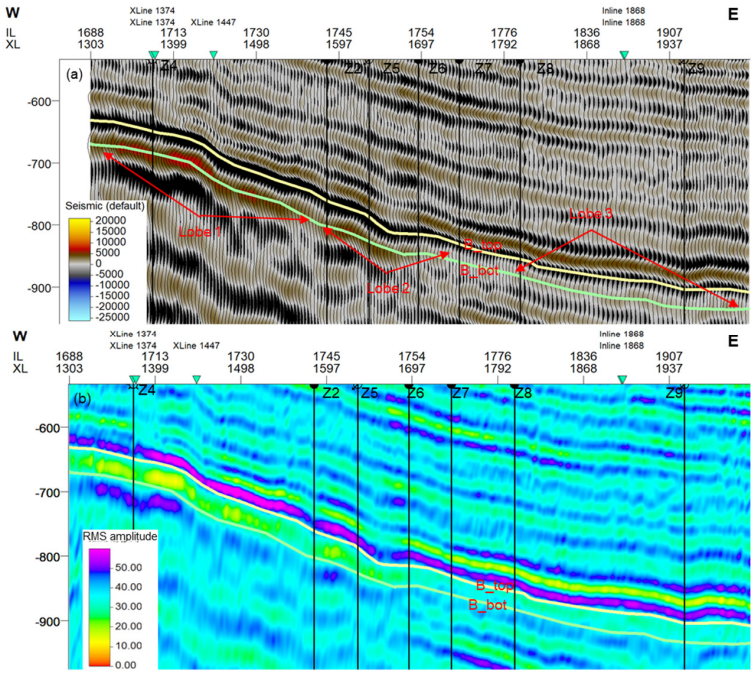


Figure 6. Features of turbidite lobes in seismic data. (**a**) The seismic data for well section of Z4–Z9; (**b**) The RMS amplitude for well section of Z4–Z9.

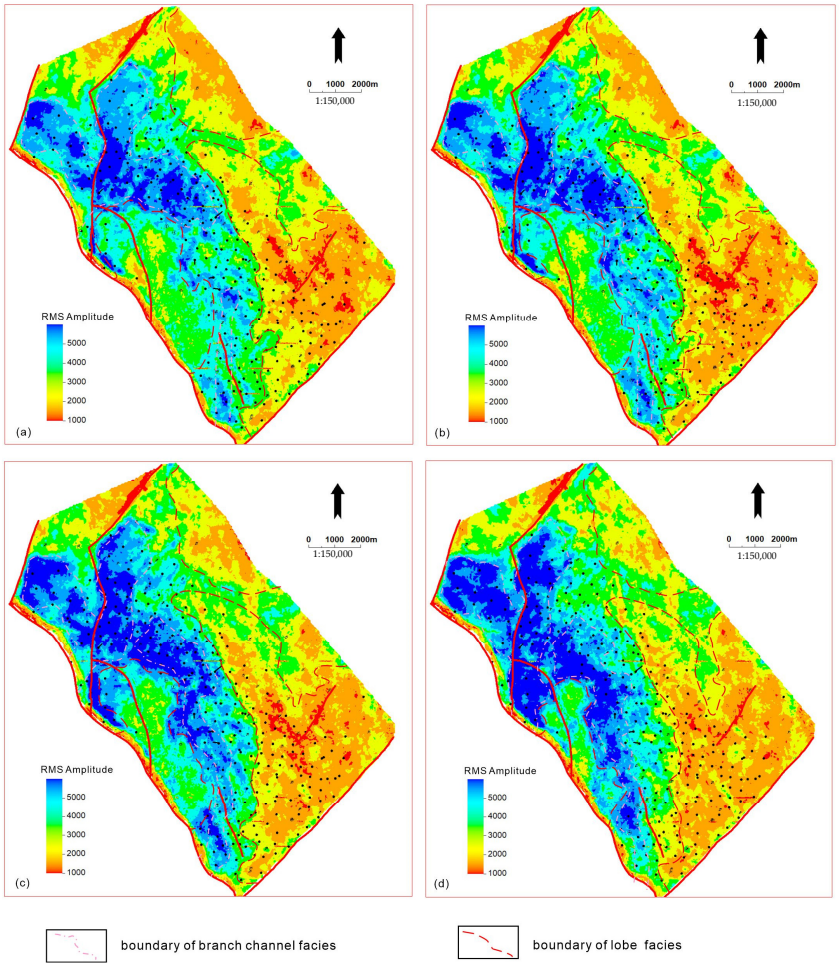


Figure 7. Sedimentary features of turbidite lobes by using seismic data. (**a**) The RMS amplitude for layer IV; (**b**) The RMS amplitude for layer III; (**c**) The RMS amplitude for layer II; (**d**) The RMS amplitude for layer I.

There are still controversies regarding the development characteristics of waterways in deep-water turbidite lobes. Duan RK et al. consider that they develop at the edge of the turbidite lobes, while Lin et al. [50] think that they develop inside the lobes and only develop in the late stage. Waterways in the study area develop simultaneously with the turbidite lobes and are relatively fixed in the depressions where the turbidite lobes are spliced. Based on the analysis of the deposition of turbidite lobes in this paper, it is considered that the feeder channels in the study area are characterized by long-term stable development at the edge of the lobes. All of them have the characteristics of undercut erosion and can develop in the early, middle, and late stages.

A comprehensive quantitative analysis was carried out on the development characteristics of the turbidite lobes and feeder channels within different stratigraphic layers of the study area (Figures 8 and 9). In the plane, within layer I2, a set of the largest lobes was identified. These lobes extend 6768 m in length (ranging from Well Z5 to Well Z9) and 3610 m in width (from Well Z2 to Well Z9) along the feeder channel. The majority of the lobes have an extension length that can reach up to 1.5 km. The feeder waterways are predominantly developed in the vicinity of Well Z2. Seismic data demonstrates that their main direction of extension is from the south to the north (Figure 7). Vertically, in the high part of the structure, the degree of fusion among different lobes is remarkably high, with almost no discernible mudstone interlayers. The off-axis lobes facies have an average thickness of 4.28 m, yet the thickness varies significantly, spanning from 0.42 m to 10.06 m. Among the layers, layer IV has the largest average thickness, reaching 7.09 m, while layer III has the smallest average thickness, merely 1.72 m. The lobe fringe facies are relatively thin, with an average thickness of 2.34 m, and its thickness ranges from 1.22 m to 3.99 m (Table 2).

Table 2. Statistics of architectural elements in different layers in Z Oilfield.

Architectural Element	Layer	Sand Number	Average Thickness/m	Maximum Thickness/m	Minimum Thickness/m	Proportion
Off-axis lobe facies	IV	14	7.82	10.06	5.41	96.99%
	III	5	1.46	2.83	0.06	43.97%
	II2	9	4.74	8.45	1.64	77.21%
	II1	11	4.41	7.04	2.81	86.67%
	I2	9	3.64	6.69	1.35	66.75%
	I1	12	3.69	6.09	0.42	86.40%
	Total	60	4.67	10.06	0.06	83.96%
Lobe fringe facies	IV	1	3.40	3.40	3.40	3.01%
	III	8	1.16	3.11	0.09	56.03%
	II2	5	2.12	2.88	1.58	19.17%
	II1	3	1.99	2.33	1.53	10.65%
	I2	5	3.09	3.93	2.24	31.42%
	I1	3	2.32	2.69	1.90	13.60%
	Total	25	1.96	3.93	0.09	14.72%
Feeder channel facies	IV	0	—	—	—	0.00%
	III	0	—	—	—	0.00%
	II2	1	2.00	2.00	2.00	3.62%
	II1	1	1.50	1.50	1.50	2.68%
	I2	1	0.90	0.90	0.90	1.83%
	I1	0	—	—	—	0.00%
	Total	3	1.47	2.00	0.90	1.32%

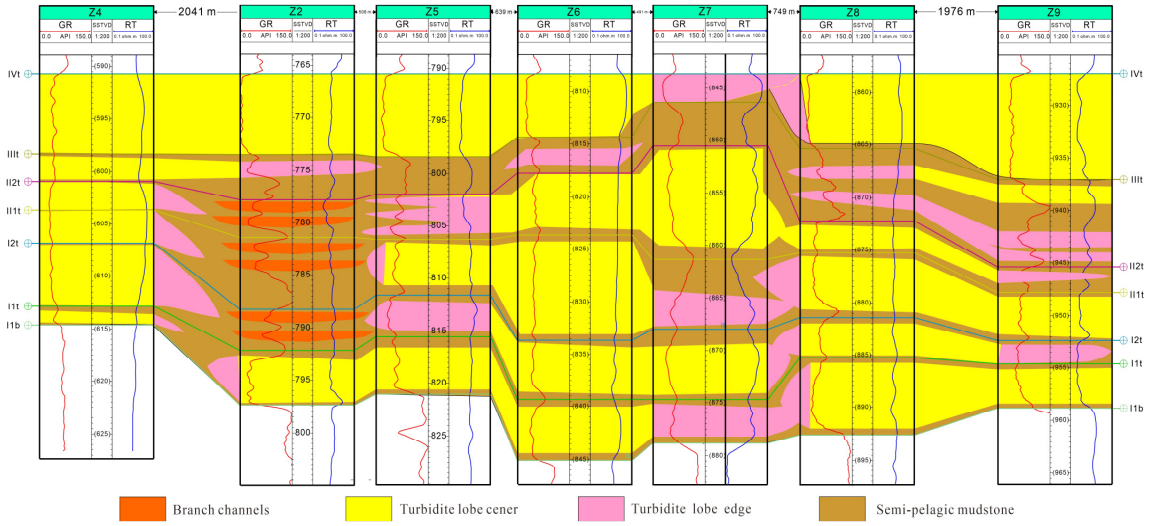


Figure 8. Reservoir architecture in the perpendicular source direction in Formation B of Z Oilfield.

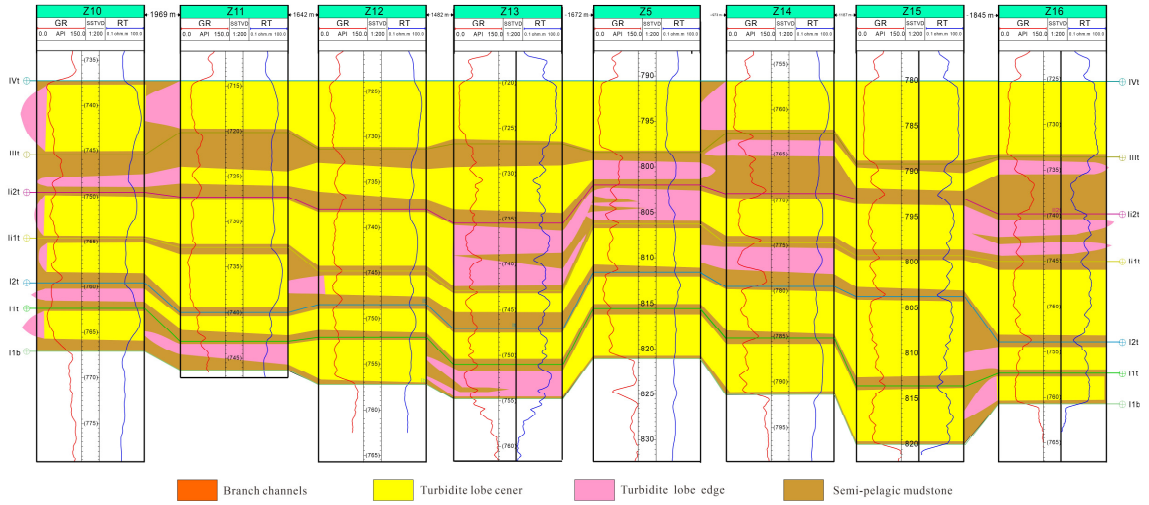


Figure 9. Reservoir architecture along the source direction in Formation B of Z Oilfield.

When compared with the off-axis lobes facies, a typical characteristic of the lobe fringe facies is its thinner thickness. Moreover, the lobe fringe facies are distinctively characterized by the lateral splitting of a single sand body into multiple sets of thin sandstone–mudstone interbeds. The feeder channel has an average sand thickness of only 1.75 m and contains numerous clay interlayers. This indicates that the hydrodynamic force within the channel experiences rapid changes and persists over a relatively long period (Table 2).

4.3. Study on Distribution of Remaining Oil

Although some new methods have been put forward to describe the remaining oil in recent years [56], reservoir simulation is still the most important method to study the remaining oil. Based on the results of reservoir architecture analysis, a three-dimensional geological model was established in conjunction with the development characteristics of turbidite lobes. Considering the relatively stable distribution of turbidite lobes and the abundant well data, a three-dimensional fine geological model of reservoirs can be built through sequential Gauss interpolation between wells based on the research results of reservoir architecture [57]. This model depicts the quantitative characterization of the shape, extension direction, scale, spatial architecture relationship, and reservoir petrophysical parameters of the turbidite lobes. Numerical simulation was carried out based on the

three-dimensional model, which integrates actual reservoir parameters, high-pressure physical properties, relative permeability curves, actual development strategies, and the oil–water well production system. Eventually, the distribution characteristics of the remaining oil were obtained. The study area is an oil reservoir with a gas cap and edge water. The numerical simulation results show that the remaining oil is near the gas–oil contact (Figure 10). The gas–oil contact is located at the high part of the structure, but in some areas, a turbidite off-axis lobe develops there, which is an important area for tapping potential. Layer III+IV is characterized by continuous distribution of turbidite lobes, good reservoir physical properties, continuous lateral distribution of lobes over a large area, good development effect, and limited remaining oil potential. Layer I+II is spliced by two sets of turbidite lobes, and the remaining oil is abundant at the lobe fringe. For example, Z2, Z4, Z5, and Z6 are at the boundary of splicing two turbidite lobes, and the remaining oil is relatively abundant, which is an important area for tapping potential (Figure 11).

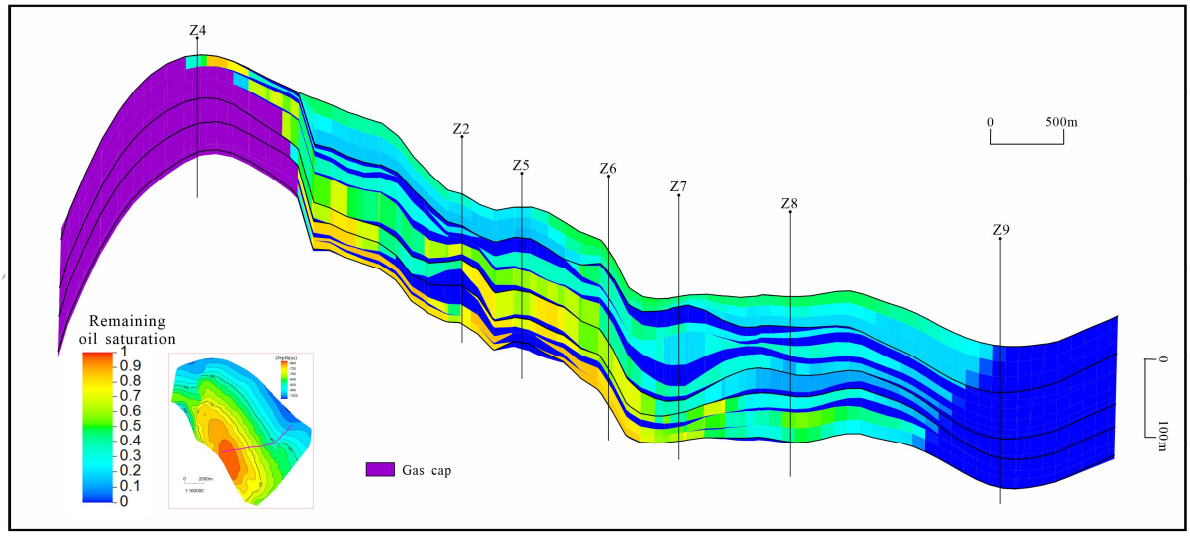


Figure 10. Numerical simulation results of profile remaining oil distribution in Z Oilfield.

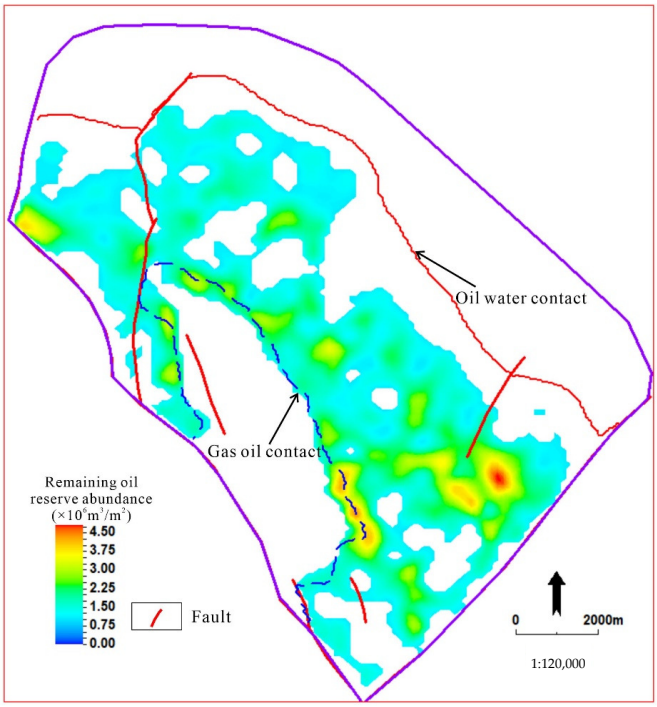


Figure 11. Numerical simulation of planar remaining oil reserve abundance in the Z Oilfield.

5. Discussion

5.1. The Sedimentary Evolution of Turbidite Lobes

Layers I to IV in the study area are deposited under the background of sea level regression. During the deposition period of layers I and II, the sea level continuously fell (Figure 3), and the channel eroded the previous sediments and transported them to the deeper water area. Meanwhile, multiple sets of lobe deposits were developed near the feeder channel, and different lobe bodies were spliced with each other to form a spatially continuous reservoir with good properties (Figures 8 and 9). During the deposition of layer III, due to a short-term rise in sea level, relatively dispersed and thin lobe deposits were formed. During the IV period, due to the lowest sea level, the accommodation space was relatively limited, and a large number of lobes moved forward and laterally, and the lobes overlapped with each other, forming large-scale continuous lobes with the average thickness of 7.8 m (Figures 8 and 9, Table 2). After the deposition of layer IV, a large-scale transgression occurred in the study area, leading to the local development of turbidite lobes and the loss of Formation V in local areas.

5.2. Influence for Water Injection

In the early stage, the study area was developed through water injection outside the oil zone. However, the reservoir production monitoring results indicated that the injected water flowed in the direction opposite to the oil zone. As a result, the oil wells within the oil zone could hardly achieve effective production, leading to an extremely poor marginal water-injection effect. The key cause lies in the fact that two sets of independent lobes were formed in the high part and low part of the structure. This geological configuration makes it arduous to effectively drive the injected water from the lower part to the higher part of the structural area. At present, the oilfield implements the point water-injection strategy, which guarantees that the injection wells and production wells are located within the same lobes. This strategy has yielded remarkable development results. The comprehensive water cut has been stably maintained below 50% for an extended period. The recovery rate has been substantially enhanced, increasing from 35.9% to 44.21%. Moreover, the formation pressure has gradually rebounded from 7.7 MPa to 9.1 MPa.

5.3. Development Strategy Based on Reservoir Architecture Features

Based on the analysis results of reservoir architecture in this paper, the gas–oil contact near the high part of the structure is a key area for tapping the potential of remaining oil. This area has good reservoirs and should be given special attention. Another key area for tapping the potential of remaining oil is the lobe fringe facies, which are formed due to poor petrophysical properties. As sandstone and mudstone are interbedded there, it is mainly considered to improve well patterns and strengthen the corresponding relationship between injection wells and production wells to effectively displace the remaining oil. For the turbidite lobes, the reservoir in the off-axis lobes facies have a large thickness and good petrophysical properties. However, for the lobe fringe facies, sandstone and mudstone are frequently interbedded, resulting in reservoir thinning and poor petrophysical properties. Thus, it is suggested to deploy water-injection wells in the off-axis lobes facies and production wells in the lobe fringe facies to ensure that the oil well has good productivity and can continuously replenish energy for the formation. The above development method can be simply summarized as “production at the off-axis lobes facies and injection at the lobe fringe facies (POIF)” (Figure 12).

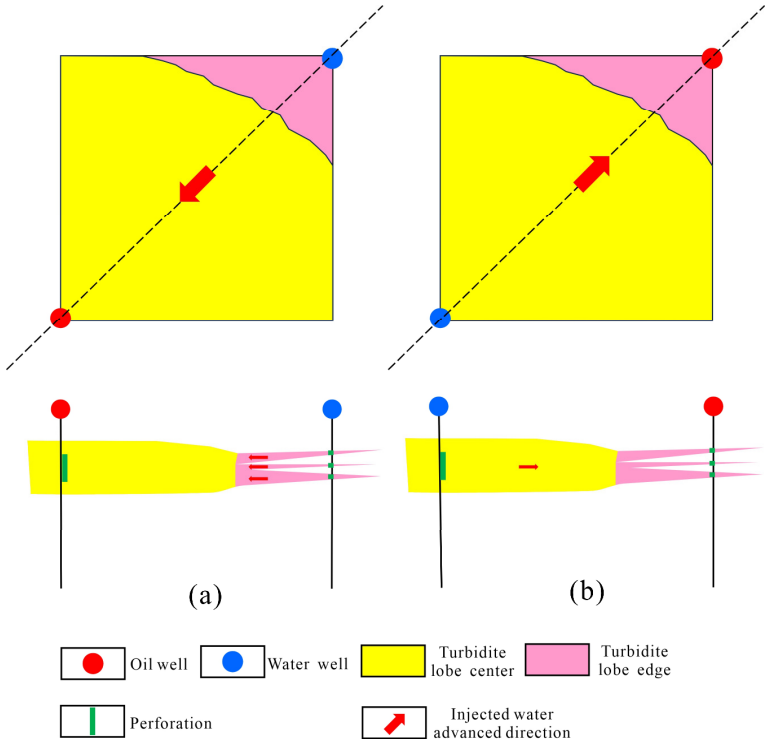


Figure 12. Development strategy for the turbidite lobes. (**a**) Production at the off-axis lobes facies and injection in the lobe fringe facies; (**b**) Production at the lobe fringe facies and injection at the off-axis lobes facies.

5.4. Analysis on the Actual Effect of the Development Strategy of "POIF"

So far, new wells have been deployed in the zone near the gas–oil contact in the high part of the structure to tap potential. The oil testing results show that the oil production can reach 130 m^3/d, which further confirms the potential in the high part near the gas–oil contact. However, there is still a lack of an effective development strategy for the remaining oil in the lobe fringe facies caused by poor petrophysical properties. In this paper, the development strategy of "POIF" is put forward, and the feasibility of this strategy is further demonstrated in detail based on the existing development data.

The Well Z18 group is one of the zones with the most abundant remaining oil in the study area. Based on the characteristics of thin deposition thickness and frequent interbedding of sandstone and mudstone, it is judged that the vicinity of this well develops the lobe fringe facies (Figure 13a,b).

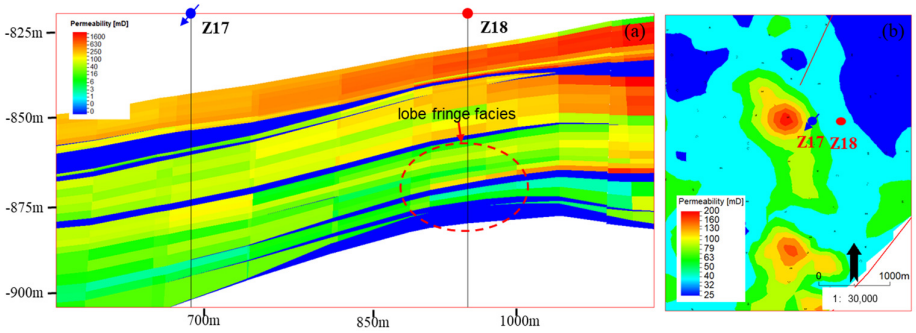


Figure 13. Distribution of reservoir permeability in Well Z18 group zone. (**a**) Sectional distribution of reservoir permeability in Well Z18 group zone; (**b**) Planar distribution of reservoir permeability in Well Z18 group zone.

Well Z18 and Z17 are the corresponding wells for production and injection. Well Z18 was completed as a production well in June 1970. Well Z17 was put into production in July 2006 and began water injection in early 2007. The injection–production relationship between Well Z18 and Well Z17 conforms to the development strategy of "POIF". Judging from the production dynamic data, it can be seen that after Well Z17 is converted to injection, the production of Well Z18 is significantly improved compared with that before the injection conversion (Figure 14).

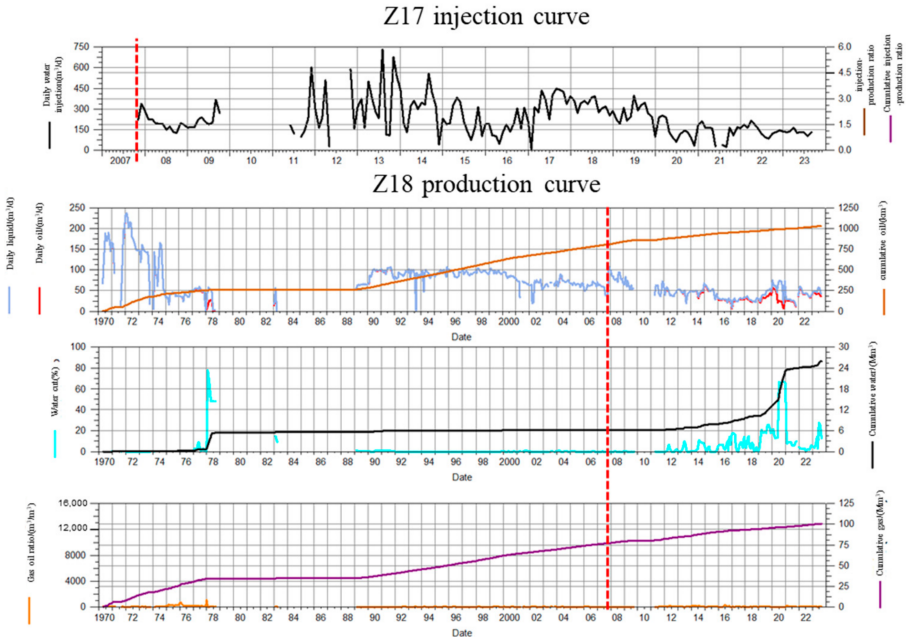


Figure 14. The corresponding relationship between injecting Well Z17 and producing Well Z18.

Based on the characteristics of thin deposition thickness and frequent interbedding of sandstone and mudstone, it is judged that the vicinity of Well Z19 is the lobe fringe facies (Figure 15). Well Z20 began to inject water in 2011. Well Z20 started production in 1985 and was shut in 2002. This well group is developed by production Well Z20 developing the off-axis lobe facies and injection Well Z19 developing lobe fringe facies. After the water injection of Well Z19 in 1991, the water cut of Well Z20 sharply rose to 90%, and the well was shut in three years later. The injection–production effect of this well group further confirms the necessity of the development strategy of "POIF" (Figure 16).

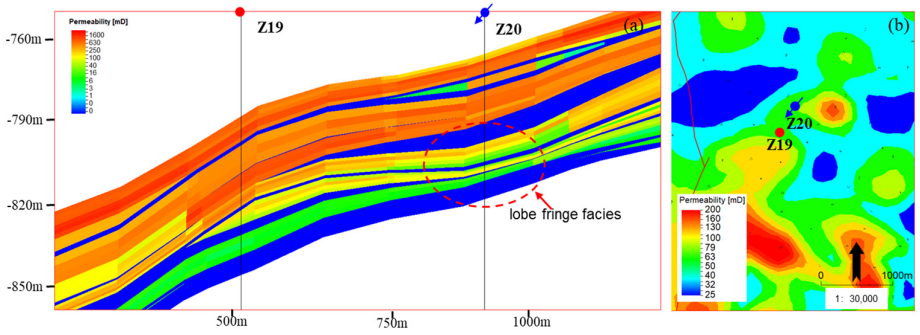


Figure 15. Distribution of reservoir permeability in Well Z19 group zone. (**a**) Sectional distribution of reservoir permeability in Well Z19 group zone; (**b**) Planar distribution of reservoir permeability in Well Z19 group zone.

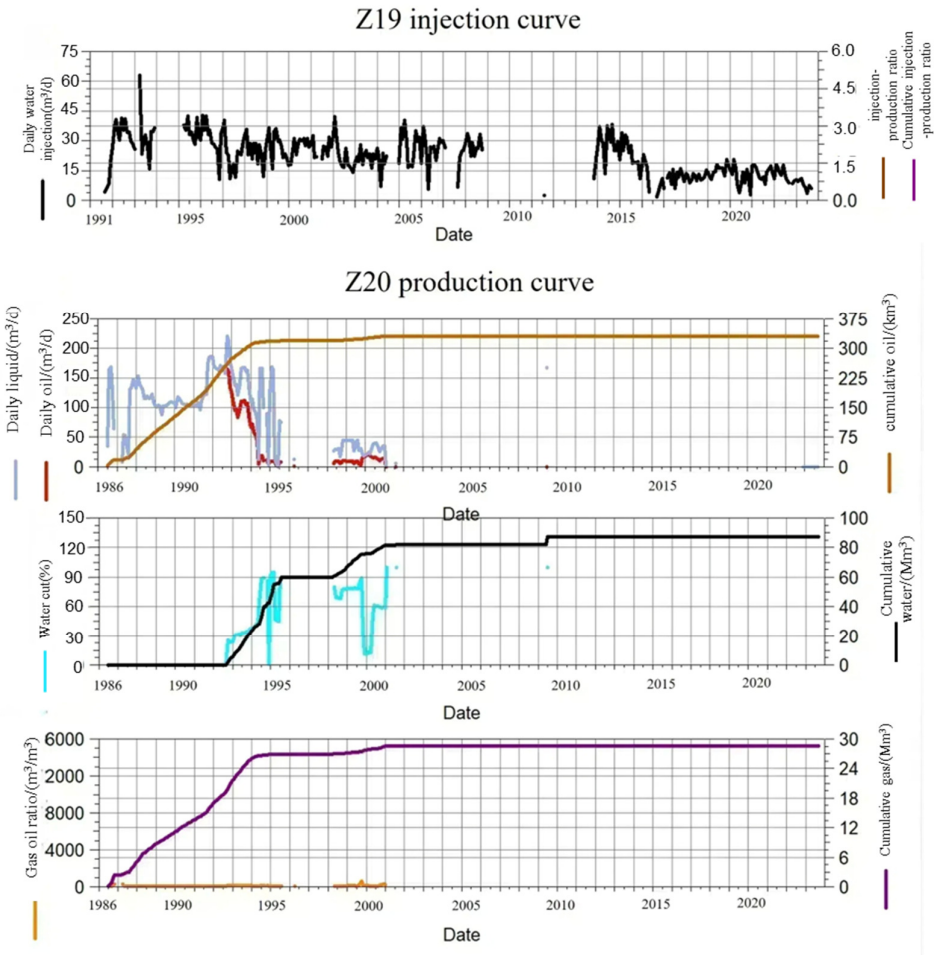


Figure 16. The corresponding relationship between injecting Well Z19 and producing Well Z20.

By comparing the production performances of Well Z18 and Well Z20, it can be observed that Well Z18, which adopts the development strategy "POIF", can boost the initial daily production of a single well by over 20 m^3. Moreover, its stable production period can be sustained for more than 3 years. In contrast, although Well Z20, employing the development strategy "production at the off-axis lobes facies and injection at the lobe fringe facies", can also increase the initial single-well production by more than 20 m^3, water breakthrough occurs merely one year later, resulting in a short stable production period. This further verifies the necessity of adopting the "POIF" development strategy.

The POIF strategy is mainly applicable to large-scale lobes developed at the termini of waterways, which can be deployed in the development well pattern. Conversely, due to the lobes developed along the lateral margins of turbidity channels being relatively small-scaled, it is difficult to effectively deploy the development well pattern, which makes it difficult to apply POIF development strategies.

6. Conclusions

Based on seismic, core, and logging data, and integrating the results of reservoir numerical simulation regarding the distribution of remaining oil, this paper comprehensively analyzes the characteristics of the reservoir architecture of turbidite lobes and puts forward corresponding development technology strategies. The conclusions are as follows:

1. A novel architecture classification scheme for turbidite lobes was proposed, which divides the reservoir architecture into seven levels. By elaborating on the scale and characteristics of reservoir architectures of different orders, this new scheme enables a

straightforward understanding of the hierarchical sequence and features of diverse reservoir architectures. This not only provides a more systematic and comprehensive framework for the study of turbidite lobe reservoir architectures but also facilitates more accurate communication and analysis within the geological research community.

2. Four distinct microfacies types are identified, including the off-axis lobe facies, the lobe fringe facies, the interlobe facies, and the feeder channels facies. The logging characteristics of these four microfacies, as well as the methods for their identification using logging data, are clarified. For the off-axis lobe facies, the GR curve exhibits a box-shaped profile with medium to high amplitude values. Notably, this curve is relatively smooth, characterized by only a few minor serrations. The lobe fringe facies, when represented on the GR curve, display either box-shaped or finger-shaped patterns. In terms of the feeder channels, the hydrodynamic gentle channels manifest as finger-shaped features on the GR curve.
3. A detailed analysis is conducted on the quantitative distribution characteristics of the turbidite lobe. The largest turbidite lobe within the study area measures 6768 m in length and 3610 m in width along the axis of the feeder channel. The majority of the turbidite lobes exhibit an extension length reaching up to 1.5 km. The feeder channels predominantly extend in a south-to-north direction, which is a crucial factor influencing the distribution and geometry of the turbidite lobes. In the high part of the structure, the interlayers between different strata are poorly developed. In contrast, in other regions of the study area, relatively stable interlayers are present.
4. The distribution of remaining oil is markedly influenced by the well patterns and reservoir architecture. The areas proximate to the oil–gas contact in the high part of the structure, as well as the junctions of two turbidite lobes, constitute the remaining oil enrichment zones. The region adjacent to the oil–gas contact in the high part of the structure represents a key area for exploiting the remaining oil potential. This area is characterized by favorable reservoir conditions, making it a prime candidate for priority potential tapping. Nevertheless, the joints of some turbidite lobes exhibit poor petrophysical properties. Such sub-optimal petrophysical characteristics can impede fluid flow and hydrocarbon recovery. Therefore, it is recommended to implement the "POIF" development strategy to maximize oil recovery.

Author Contributions: Conceptualization, C.L. and W.L.; methodology, C.L.; software, H.Y.; validation, Q.Z., X.S. and S.W.; formal analysis, C.L. and X.Z.; investigation, C.L.; resources, H.Y., Q.Z., X.S. and S.W.; data curation, H.Y., Q.Z., X.S., H.W., Z.Z. (Zhaofeng Zhu) and S.W.; writing—original draft preparation, C.L. and W.L.; writing—review and editing, D.W., H.W., Z.Z. (Zhaofeng Zhu), X.Z. and Z.Z. (Ziyu Zhang); visualization, D.W. and Z.Z. (Ziyu Zhang); supervision, H.Y.; project administration, W.L.; funding acquisition, W.L. All authors have read and agreed to the published version of the manuscript.

Funding: This work was supported by the PetroChina Company Limited International Science and Technology Cooperation Project (2021DQ0403) and CNPC Research on Key Technologies for Overseas Deepwater Oil and Gas Field Exploration and Development Projects (2023-SC-01-03).

Data Availability Statement: Data available on request from the authors.

Acknowledgments: The authors would like to thank the anonymous reviewers for their comments and very helpful suggestions.

Conflicts of Interest: Authors Changhai Li, Huimin Ye, Qiang Zhu, Xuejun Shan, Shengli Wang, Deyong Wang, Xianjie Zhou and Zhaofeng Zhu were employed by the company Sinopec International Petroleum Exploration and Development Corporation. The remaining author declares that the research was conducted in the absence of any commercial or financial relationships that could be construed as a potential conflict of interest.

References

1. Miall, A.D. Architectural-element analysis: A new method of facies analysis applied to fluvial deposits. *Earth-Sci. Rev.* **1985**, *22*, 261–308. [CrossRef]
2. Miall, A.D.; Jones, B.G. Fluvial architecture of the Hawkesbury sandstone (Triassic), near Sydney, Australia. *J. Sediment. Res.* **2003**, *73*, 531–545. [CrossRef]
3. Jamil, M.; Siddiqui, N.A.; Rahman AH, B.A.; Ibrahim, N.A.; Ismail MS, B.; Ahmed, N.; Usman, M.; Gul, Z.; Imran, Q.S. Facies heterogeneity and lobe facies multiscale analysis of deep-marine sand-shale complexity in the West Crocker Formation of Sabah Basin, NW Borneo. *Appl. Sci.* **2021**, *11*, 5513. [CrossRef]
4. Mueller, P.; Patacci, M.; Di Giulio, A. Hybrid event beds in the proximal to distal extensive lobe domain of the coarse-grained and sand-rich Bordighera turbidite system (NW Italy). *Mar. Pet. Geol.* **2017**, *86*, 908–931. [CrossRef]
5. Zakaria, A.A.; Johnson, H.D.; Jackson, C.A.; Tongkul, F. Sedimentary facies analysis and depositional model of the Palaeogene West Crocker submarine fan system, NW Borneo. *J. Asian Earth Sci.* **2013**, *76*, 283–300. [CrossRef]
6. Bourget, J.; Zaragosi, S.; Mulder, T.; Schneider, J.-L.; Garlan, T.; Van Toer, A.; Mas, V.; Ellouz-Zimmermann, N. Hyperpycnal-fed turbidite lobe architecture and recent sedimentary processes: A case study from the Al Batha turbidite system, Oman margin. *Sediment. Geol.* **2010**, *229*, 144–159. [CrossRef]
7. Doughty-Jones, G.; Mayall, M.; Lonergan, L. Stratigraphy, facies, and evolution of deep-water lobe complexes within a salt-controlled intraslope minibasin. *AAPG Bull.* **2017**, *101*, 1879–1904. [CrossRef]
8. Zhang, L.; Yilong, L. Architecture of deepwater turbidite lobes: A case study of Carboniferous turbidite outcrop in the Clare Basin, Ireland. *Pet. Explor. Dev.* **2020**, *47*, 990–1000. [CrossRef]
9. Duan, R.K.; Zhang, X.; Guo FXChen, G.N.; Hu, G.Y.; Zou, J.Y. Internal sedimentary structure and stacking patterns of deep-water lobe complex: A case study of Miocene zone D in Akpo oilfield, Niger Delta Basin. *Lithol. Reserv.* **2022**, *34*, 110–120.
10. Spychala, Y.T.; Hodgson, D.M.; Lee, D.R. Autogenic controls on hybrid bed distribution in submarine lobe complexes. *Mar. Pet. Geol.* **2017**, *88*, 1078–1093. [CrossRef]
11. Prelat, A.; Covault, J.A.; Hodgson, D.M.; Fildani, A.; Flint, S.S. Intrinsic controls on the range of volumes, morphologies, and dimensions of submarine lobes. *Sediment. Geol.* **2010**, *232*, 66–76. [CrossRef]
12. Zhang, J.J.; Wu, S.H.; Fan, T.E.; Fan, H.J.; Jiang, L.; Chen, C.; Wu, Q.; Lin, P. Research on the architecture of submarine-fan lobes in the Niger Delta Basin, offshore West Africa. *J. Palaeogeogr.* **2016**, *5*, 185–204. [CrossRef]
13. Siddiqui, N.A.; Ramkumar, M.; Rahman AH, A.; Mathew, M.J.; Santosh, M.; Sum, C.W.; Menier, D. High resolution facies architecture and digital outcrop modeling of the Sandakan formation sandstone reservoir, Borneo: Implications for reservoir characterization and flow simulation. *Geosci. Front.* **2019**, *10*, 957–971. [CrossRef]
14. Groenenberg, R.M.; Hodgson, D.M.; Prelat, A.; Luthi, S.M.; Flint, S.S. Flow–deposit interaction in submarine lobes: Insights from outcrop observations and realizations of a process-based numerical model. *J. Sediment. Res.* **2010**, *80*, 252–267. [CrossRef]
15. Macdonald, H.A.; Peakall, J.; Wignall, P.B.; Best, J. Sedimentation in deep-sea lobe-elements: Implications for the origin of thickening-upward sequences. *J. Geol. Soc.* **2011**, *168*, 319–332. [CrossRef]
16. Starek, D.; Fuksi, T. Distal turbidite fan/lobe succession of the Late Oligocene Zuberec Fm.–architecture and hierarchy (Central Western Carpathians, Orava–Podhale basin). *Open Geosci.* **2017**, *9*, 385–406. [CrossRef]
17. Spychala, Y.T.; Hodgson, D.M.; Prélat, A.; Kane, I.A.; Flint, S.S.; Mountney, N.P. Frontal and lateral submarine lobe fringes: Comparing sedimentary facies, architecture and flow processes. *J. Sediment. Res.* **2017**, *87*, 75–96. [CrossRef]
18. Zhang, J.; Wu, S.; Hu, G.; Fan, T.E.; Yu, B.; Lin, P.; Jiang, S. Sea-level control on the submarine fan architecture in a deepwater sequence of the Niger Delta Basin. *Mar. Pet. Geol.* **2018**, *94*, 179–197. [CrossRef]
19. Fuhrmann, A.; Kane, I.A.; Schomacker, E.; Clare, M.A.; Pontén, A. Bottom current modification of turbidite lobe complexes. *Front. Earth Sci.* **2022**, *9*, 752066. [CrossRef]
20. Gervais, A.; Savoye, B.; Mulder, T.; Gonthier, E. Sandy modern turbidite lobes: A new insight from high resolution seismic data. *Mar. Pet. Geol.* **2006**, *23*, 485–502. [CrossRef]
21. Kuswandaru, G.Y.; Amir Hassan, M.H.; Matenco, L.C.; Taib, N.I.; Mustapha, K.A. Turbidite, debrite, and hybrid event beds in submarine lobe deposits of the Palaeocene to middle Eocene Kapit and Pelagus members, Belaga Formation, Sarawak, Malaysia. *Geol. J.* **2019**, *54*, 3421–3437. [CrossRef]
22. Zhang, L.F.; Dong, D.Z. Thickening-upward cycles in deep-marine and deep-lacustrine turbidite lobes: Examples from the Clare Basin and the Ordos Basin. *J. Palaeogeogr.* **2020**, *9*, 1–16.
23. Mutti, E.; Bernoulli, D.; Lucchi, F.R.; Tinterri, R. Turbidites and turbidity currents from Alpine 'flysch'to the exploration of continental margins. *Sedimentology* **2009**, *56*, 267–318. [CrossRef]
24. Liu, Q.; Kneller, B.; Fallgatter, C.; Buso, V.V. Quantitative comparisons of depositional architectures of unconfined and con-fined turbidite sheet systems. *Sediment. Geol.* **2018**, *376*, 72–89. [CrossRef]
25. Scacchia, E.; Tinterri, R.; Gamberi, F. Downslope evolution of supercritical bedforms in a confined deep-sea fan lobe, Amantea Fan, Paola Basin (Southeastern Tyrrhenian Sea). *Sediment. Geol.* **2024**, *466*, 106636. [CrossRef]

26. Łapcik, P. Distribution of transitional flow deposits in sedimentary environments of mixed sand-mud turbidite system. *Sediment. Geol.* **2024**, *473*, 106766. [CrossRef]
27. Gonçalves, L.A.; Arienti, L.M.; D'Ávila, R.F.S.; Carbone, O.C.; Ribeiro, A. High-resolution sequence stratigraphy applied to turbidites: The case study of Jurassic Los Molles Formation, Neuquén Basin, Argentina. *J. South Am. Earth Sci.* **2022**, *120*, 104078. [CrossRef]
28. Cabrera-Ortiz, J.F.; Dorador, J.; Rodríguez-Tovar, F.J.; Pérez-Asensio, J.N. Paleoenvironmental conditions and evolution of a muddy turbidite system: An integrated sedimentological and ichnological analysis. *J. Sediment. Res.* **2025**, *95*, 86–103. [CrossRef]
29. Fernandes FJ, D.; de Oliveira Neto, E.R.; Teixeira, L.; Freire AF, M.; Lupinacci, W.M. Cycle-consistent convolutional neural network for seismic impedance inversion: An application for high-resolution characterization of turbidites reservoirs. *Geoenergy Sci. Eng.* **2024**, *235*, 212709. [CrossRef]
30. Obafemi, S.; Oyedele, K.; Omeru, T.; Bankole, S.; Opatola, A.; Pat-Nebe, O.; Akinwale, R.; Ademilola, J.; Adebayo, R.; Victor, A.L. 3D facies and reservoir property prediction of deepwater turbidite sands; case study of an offshore Niger delta field. *J. Afr. Earth Sci.* **2022**, *194*, 104633. [CrossRef]
31. Olagundoye, O.; Akhajeme, E.; Yusuf, M.; Chizea, C.; Spina, V.; Joubert, T.; Parsa, A.; Fashanu, M.; Enuma, C.; Jaiyeola, J.; et al. Seismic net-to-gross estimation for a geologic model update: A case study from a turbidite lobe reservoir in the deepwater of the Niger Delta. *Interpretation* **2024**, *12*, SE35–SE53. [CrossRef]
32. Alpak, F.O.; Xue, G. Effects of fine-scale turbidite lobe stratigraphic architecture on dynamic reservoir performance. *Mar. Pet. Geol.* **2022**, *139*, 105540. [CrossRef]
33. Lim, H.G.; Lee, C. Reservoir connectivity in deep-water turbidite deposits over geological and production time scales: An integrated study of the Shwe field, Bay of Bengal. *J. Pet. Explor. Prod. Technol.* **2024**, *14*, 3349–3366. [CrossRef]
34. da Silveira, A.S.; Cardoso Jr, M.; Paim, P.S.; Faccion, J.E.; D'Ávila, R.S.; Leanza, H. 3D stochastic simulation of a deep-water turbidite system: An exam-ple from the Los Molles Formation, southern region of the Neuquén Basin, Argentina. *J. South Am. Earth Sci.* **2024**, *149*, 105229. [CrossRef]
35. Xu, R.; Zhang, W.; Li, M.; Lu, W. A multiple-point stochastic-based turbidite lobe architecture geomodeling: A case study from L Oilfield, Lower Congo Basin, West Africa. *Interpretation* **2023**, *11*, B1–B13. [CrossRef]
36. Ji, C.H. *Sequence Stratigraphy and Sedimentary Facies Analysis in Layer F4 of Zarzaitine Oil Field*; China University of Geoscience: Beijing, China, 2011; pp. 1–79.
37. Zhang, Z.M.; Li, Y.F.; Zheng, N.X.; Cao, Z.; Lu, X.Y.; Li, Z.F.; Sun, R.M.; Xia, C.S.; Li, L.; Niu, B.; et al. Early Paleozoic lithofacies palaeogeography evolution characteristics of Ghadames Basin in North Africa. *J. Palaeogeogr.* **2024**, *26*, 45–57.
38. Li, S.M. Sedimentary microfacies modelling for submarine fan in Zarzaitine Oilfield. *Fault Block Oil Gas Field* **2007**, *14*, 31–33.
39. Li, S.M.; Deng, H.W.; Wu, X. Sedimentary characteristics and evolution of Lower Devonianin Zarzaitine Oilfield, Eastern Algeria. *Pet. Explor. Dev.* **2006**, *03*, 383–387.
40. Sun, G.J. *Enhanced Oil Recovery Technology Research and Application of F4 Reservoir in Zarzaitine Oilfield in Algeria*; China University of Geoscience: Beijing, China, 2013; pp. 1–47.
41. Jennette, D.; Wawrzyniec, T.; Fouad, K.; Dunlap, D.B.; Meneses-Rocha, J.; Grimaldo, F.; Muñoz, R.; Barrera, D.; Williams-Rojas, C.T.; Escamilla-Herrera, A. Traps and turbidite reservoir characteristics from a complex and evolving tectonic setting, Veracruz Basin, southeastern Mexico. *AAPG Bull.* **2003**, *87*, 1599–1622. [CrossRef]
42. Huang, Y. Sedimentary characteristics of turbidite fan and its implication for hydrocarbon exploration in Lower Congo Basin. *Pet. Res.* **2018**, *3*, 189–196. [CrossRef]
43. Huang, Y.; Tan, X.; Liu, E.; Wang, J.; Wang, J. Sedimentary processes of shallow-marine turbidite fans: An example from the Huangliu Formation in the Yinggehai Basin, South China Sea. *Mar. Pet. Geol.* **2021**, *132*, 105191. [CrossRef]
44. Zheng, W.B.; Wu, X.L.; Deng, H.W. Stratigraphy and Facies Distribution of Lower Devonian F4 Unit in Zarzaitine Oilfield, Illizi Basin, Algeria. *Earth Sci. J. China Univ. Geosci.* **2012**, *37*, 181–190.
45. Galeazzi, S.; Point, O.; Haddadi, N.; Mather, J.; Druesne, D. Regional geology and petroleum systems of the Illizi–Berkine area of the Alge-rian Saharan Platform: An overview. *Mar. Pet. Geol.* **2010**, *27*, 143–178. [CrossRef]
46. Li, L. Study on Heterogeneity of F4 Reservoir in Zarzaitine Oilfield. *China Acad. J. Electron. Publ. House* **2012**, *10*, 114.
47. English, K.L.; Redfern, J.; Corcoran, D.V.; English, J.M.; Cherif, R.Y. Constraining burial history and petroleum charge in exhumed basins: New insights from the Illizi Basin, Algeria. *AAPG Bull.* **2016**, *100*, 623–655. [CrossRef]
48. Mutti, E.; Normark, W.R. Comparing examples of modern and ancient turbidite systems: Problems and concepts. In *Marine Clastic Sedimentology: Concepts and Case Studies*; Springer: Dordrecht, The Netherlands, 1987; pp. 1–38.
49. Lamb, M.A.; Anderson, K.S.; Graham, S.A. *Stratigraphic Architecture of a Sand-Rich, Deep-Sea Depositional System: The Stevens Sandstone, San Joaquin Basin, California*; Pacific Section American Association of Petroleum Geologists: Tulsa, OK, USA, 2003; Volume MP-47.
50. Lin, Y.; Wu, S.H.; Wang, X.; Zhao, X.M.; Ling, Y.; Lu, Y.; Zhang, J.J. Research on reservoir architecture models of deep-water turbidite lobes. *Nat. Gas Geosci.* **2014**, *25*, 1197–1204.

51. Yu, J.; Song, Y.; Shi, K.; Chen, S.; Wang, Q.; Liu, B.; Han, J. Depositional facies and sequence architecture of the Yijianfang Formation in the Shuntuoguole Low Uplift, Tarim Basin, NW China. *Geol. J.* **2022**, *57*, 3135–3157. [CrossRef]
52. Zhenzhen, J.; Chengyan, L.; Guanghui, Y. Wavelet analysis models based on high resolution sequence stratigraphy. *Geoscience* **2013**, *27*, 397.
53. Meyers, S.D.; Kelly, B.G.; O'Brien, J.J. An introduction to wavelet analysis in oceanography and meteorology: With ap-plication to the dispersion of Yanai waves. *Mon. Weather. Rev.* **1993**, *121*, 2858–2866. [CrossRef]
54. Xu, J.L.; Wang, G.W.; Liu, L.F.; Zhang, C.H.; Xue, Z.A. Application of Hilbert-Huang transform to study classification and correlation of isochrone substratum. *Oil Geophys. Prospect.* **2010**, *45*, 423–430.
55. Wu, X.L.; Zheng, W.B.; Deng, H.W. Stratigraphy and Distribution of Gravity Flow Deposition, Lower Devonian F4 Unit, Zarzaitine Oilfield, Illizi Basin, Algeria. *Pet. Sci. Technol.* **2012**, *30*, 1151–1162. [CrossRef]
56. Martirosyan, A.; Ilyushin, Y.; Afanaseva, O.; Kukharova, T.; Asadulagi, M.; Khloponina, V. Development of an Oil Field's Conceptual Model. *Int. J. Eng.* **2025**, *38*, 381–388. [CrossRef]
57. Kim, M.; Kim, H.; Chung, C. A three-dimensional geotechnical spatial modeling method for borehole dataset using optimization of geostatistical approaches. *KSCE J. Civ. Eng.* **2020**, *24*, 778–793. [CrossRef]

Disclaimer/Publisher's Note: The statements, opinions and data contained in all publications are solely those of the individual author(s) and contributor(s) and not of MDPI and/or the editor(s). MDPI and/or the editor(s) disclaim responsibility for any injury to people or property resulting from any ideas, methods, instructions or products referred to in the content.